

Recognition of Sintering State in Rotary Kiln Using a Robust Extreme Learning Machine

Hua Chen, Jing Zhang and Hongping Hu
School of Information Science and Engineering
Hunan University
ChangSha, China
anneychen@126.com

Xiaogang Zhang*
College of Electrical and Information Engineering
Hunan University
ChangSha, China
zhangxg@hnu.edu.cn

Abstract—Sintering is a key process for the industrial clinker production. The sintering state estimation in clinker is an essential factor for its process control. In this paper, a feature extraction method from flame image and a robust extreme learning machine (RB-ELM) classifier are provided to recognize sintering process in rotary kiln. After a preprocessing of image denoising and illumination compensation, material region of flame image is segmented by region growing algorithm and a 5-D statistic feature vector is extracted from it for the following classifier. In order to reduce the influence of outliers in training data caused by blurring image and to achieve a real-time application on site, a robust extreme learning machine, which adopted iterative weight least square (IWLS) method based on M-estimator, is used for fast classification of sintering state. Experimental results show that the proposed method can recognize sintering state accurately, quickly and robustly.

Keywords—rotary kiln; vision detection; extreme learning machine; robust estimation; flame image

I. INTRODUCTION

Rotary kilns are widely used in nonferrous metallurgy, cement and other industry. The sintering state estimation of clinker in rotary kiln is very essential in production control process, which can directly influence the quality of products, energy consumption and pollutant emission level. Traditionally, the sintering state of materials in kiln can be divided into three categories: 1) normal sintering, 2) oversintering, and 3) undersintering. Normal sintering materials are qualified products and others are unqualified.

The kiln typically consists of a refractory steel cylinder of diameter 4-5m with a ratio of length to diameter greater than 20m. It is inclined along its length at an angle to the horizontal of a few degrees and rotate about its axis slowly at a rotation speed ω about 1 rev per 60-80 seconds [1]. The raw material and coal powder are fed into the kiln from the feed port of the cylinder. Sintering procedure is finished in kiln with the revolution of cylinder, and the clinker flows continuously to the discharge port through the inclination and rotation of the cylinder. The kiln is filled with material generally less than 30% by volume. The motion of granular in the kiln flow

through the cylinder is shown in Fig.1 [1].

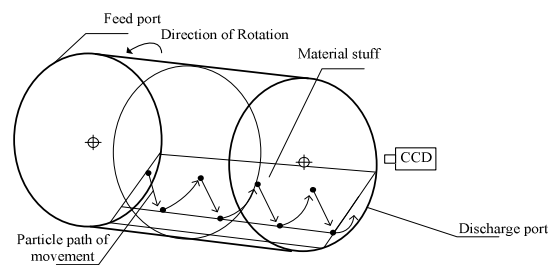


Fig. 1. Motion of granular in the kiln.

For a long time the sintering state of material is observed by operator in a manual mode. Recently, combining image analysis and machine learning algorithms to detect burning condition and control coal-feeding of rotary kiln have received more and more significant attentions. The camera locates in the discharge port of kiln and the image captured by it is shown in Fig.2. Lin [2] et al. calculated the 1-4 order statistic HSI data of rotary kiln flame image to establish the identification model for combustion condition using multivariate regression method. By Gabor wavelet based texture coarseness and Fuzzy C-Means cluster algorithm Sun [3] et al. proposed an improved segmentation method for flame image of rotary kiln burning region. He [4] et al. calculated the Grey-Level Co-occurrence Matrix (GLCM) texture features of clinker region and classified the sintered clinkers to different qualities. Zhang [5] et al. realized a content-based retrieval system for kiln sintering region flame image by the texture and fire features of it. Li [6] et al. used a set of heterogeneous features and fusion techniques to construct a flame-based sintering state recognition system. The flame images captured by the digital camera were always partitioned to several regions such as coal region, bright region and material region et al (Fig.2). The above mentioned methods mostly extract various features such as HSI, texture feature and so on from the segmented regions. Fig. 3. is the typical flame image sequence captured from the rotary kiln of a large alumina plant. Because of illumination and fog in kiln, the image is so blurring that it is difficult to segment material zone, and extracting texture feature from it is even more impossible. So the sintering state detection methods mentioned above can not work well in blurring flame image. On the other hand, the above methods

* Corresponding Author.

This work was supported by National Natural Science Foundation of China (No. 61203016, No.61174050, No. 61174140).

are lack of efficient and real-time ability because of complex classifier and feature computing.

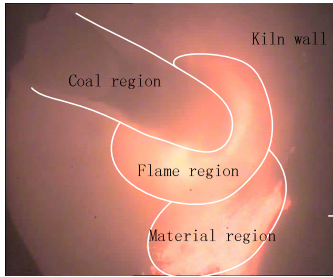


Fig. 2. Rotary kiln axial fuzzy video images.

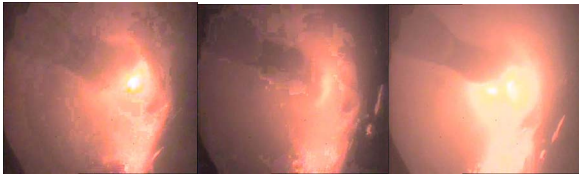


Fig. 3. Flame image sequence captured in sintering area of rotary kiln.

In this paper, a new feature extraction method and fast robust classifier are presented to recognize the sintering state in rotary kiln based on blurring flame images. After an image preprocessing for noise removal and illumination compensation, material region is segmented by region growing algorithm and a 5-D statistic feature vector is extracted from it as the inputs to the classifier. Subsequently, a robust extreme learning machine (RB-ELM) is used to recognize the sintering state with the features, which has not only shorter training time for real-time application than other classifiers, but also has robust abilities to overcome the negative influence of outliers in feature caused by blurring image on site.

The rest of the paper is organized as follows. In Section II, the preprocessing procedure, material region segmentation, and feature extraction are described. Section III describes the robust extreme learning machine algorithm. Section IV presents its results and compares them to other classification methods. Finally, the authors' conclusions and discussion conclude this paper.

II. PROPOSED PREPROCESSING, SEGMENTATION AND FEATURE EXTRACTION METHOD

This section presents the proposed preprocessing procedure, material region segmentation and feature extraction methods. The following process stages may be identified: 1) original blurring image preprocessing, 2) material region segmentation and postprocessing, and 3) statistic feature extraction for sintering state classification.

A. Preprocessing

Processed images I_g are monochrome and obtained by extracting the green band from original RGB kiln sintering images. The green channel provides the best contrast of the RGB representation (Fig. 4).

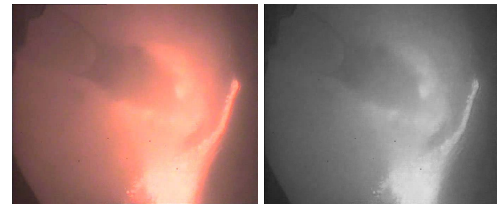


Fig. 4. RGB image and green channel image.

Because of the burning of material the kiln sintering images represent serious illumination variation, and the ROI is difficult to be segmented. We use Fuzzy C-Means (FCM) [7] and region growing algorithm [8] to segment the material region, the results are shown in Fig.5. It is failed to segment the material region correctly because of uneven illumination in kiln. So, a preprocessing procedure comprising noise removal and background homogenization is applied.

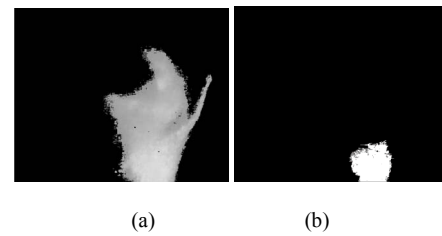


Fig. 5. Segmentation result without preprocessing: (a) FCM segmentation image (b) region growing segmentation image

A 7×7 median filter is applied to eliminate occasional salt-and-pepper noise. Further noise smoothing is performed by convolving the resultant image with a Gaussian kernel of dimensions $m \times m = 9 \times 9$, mean $\mu = 0$ and variance $\sigma^2 = 5^2$. The denoising image I_r is shown in Fig.6(a). To overcome the background intensity variation caused by burning of material in rotary kiln, a background image I_B , is produced by applying a 180×180 mean filter (Fig. 6(b)). The difference D between I_r and I_B is calculated for every pixel:

$$D(x, y) = I_r(x, y) - I_B(x, y) \quad (1)$$

Then a shade-corrected image I_{sc} (Fig. 6(c)) is obtained by transforming linearly values into integers covering the whole range of possible gray-levels (0-255, referred to 8-bit images). In order to reduce the influence by intensities variations between images, a homogenized image (Fig. 6(d)) is produced as follows: the histogram of I_{sc} is displaced toward the middle of the gray-scale by modifying pixel intensities according to the following gray-level global transformation function:

$$I_H(x, y) = I_{sc}(x, y) + 128 - I_{sc_max} \quad (2)$$

The variable denoted by I_{sc_max} defines the gray-level presenting the highest number of pixels in I_{sc} . Pixels in images with different illumination conditions will standardize their intensity around this value.

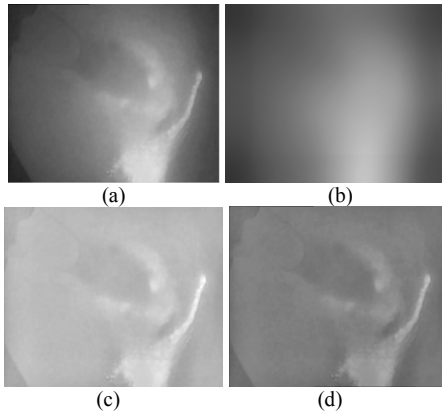


Fig. 6. Illustration of the preprocessing process: (a) Denoising result of green channel image. (b) Background image. (c) Shade-corrected image. (d) Homogenized image.

B. Material Region Segmentation and Postprocessing

After preprocessing, we use the region growing algorithm to segment material region. As mentioned above, the material region is located in the lower right side of image. Thus the region growing algorithm uses a seed point which is located in the fix position to segment the material region and gradually incorporates pixels into region R if the pixel $f(x,y)$ satisfies the similarity constraint:

$$|f(x,y) - \mu_{seed}| \leq T \quad (3)$$

$$T = \max\{I(x,y)\} - \min\{I(x,y)\} | I(x,y) \in M_s \quad (4)$$

Where $I(x,y)$ is intensities of 8 neighbors of seed point. μ_{seed} is the mean intensities of 8 neighbors of seed point. M_s is 11×11 masks with center seed. Eq. (3) and Eq. (4) are used to determine whether the region is extended. If there is no region extension, region growing is stopped.

Fig. 7(a) shows the region growing results of the I_H . To fill the hallow in the material region, a morphological closing using a 20-pixel diameter disk, defined in a square grid by using eight-connexity, as structuring element. Fig. 7(b) denotes the resultant image I_D .

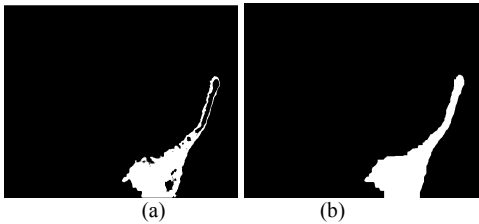


Fig. 7. Segmentation result of material region: (a) region growing result. (b) postprocessing image.

C. Feature Extraction

The aim of the feature extraction stage is the characterization of material region by means of a feature vector. The material region is represented in terms of some quantifiable measurements which may be easily used in the classification stage to decide which sintering state the current sintering material belongs to. The quality of sintering stuff can be catalogued into three groups: (1) oversintering stuff, characterized by small granularity, deep liquid phantom, and bad mobility. (2) undersintering stuff, characterized by loose granularity and over-flexible mobility. (3) normal sintering stuff, characterized by homogeneous flow, moderate granularity. The sintering state has some relation with the temperature of kiln and the gray-level of image is in proportion to the temperature. So in this paper, a set of gray-level-based statistic feature is derived from segmented images:

- 1). average gray-level of material region:

$$f_1 = \frac{1}{M} \sum_{i=1}^H f_i(x,y) \quad f_i(x,y) \in I_D \quad (5)$$

Where I_D represents the segmented material region, and M is the pixel number of material region. f_i represents the illumination intensity of material region.

- 2). average grey-level of original green band image:

$$f_2 = \frac{1}{S} \sum_{i=1}^S f_i(x,y) \quad f_i(x,y) \in I_g \quad (6)$$

Where I_g is the green channel image of original RGB color image, and S is the pixel number of green band image.

- 3). the leftmost x-coordinate of material region:

$$f_3 = x_{\min} = \min(x_1, \dots, x_i, \dots, x_n) \quad x_i \in I_D \quad (7)$$

- 4). the topmost-coordinate of material region:

$$f_4 = y_{\max} = \max(y_1, \dots, y_i, \dots, y_n) \quad y_i \in I_D \quad (8)$$

- 5) angle of centroid swing

On the basis of results of experimental study, the repose angle γ is one of the most important material properties describing the granular material motion in rotating kiln [9,10]. The value of repose angle reflects the viscosity and fluidity of stuff indirectly, which is the higher viscosity and weaker fluidity, the bigger angle of repose. In our experiment, to simplify computation complexity we use the angle of centroid swing θ to substitute for the repose angle (Fig. 8.). The angle of centroid swing means the angle between the line from material centroid to image central point and the vertical line. The angle of centroid swing is in proportion to the angle of repose and its computation is simple than the angle of repose.

$$f_s = \theta = \arctg\left(\frac{x_c - x_m}{y_c - y_m}\right) \quad (9)$$

Where x_c and y_c are x-coordinate and y-coordinate of centroid of material region, x_m , y_m are central point's coordinates of whole image.

$$x_c = \frac{\sum_{i=1}^M f_i(x, y)x_i}{\sum_{i=1}^M f_i(x, y)} \quad (10)$$

$$y_c = \frac{\sum_{i=1}^M f_i(x, y)y_i}{\sum_{i=1}^M f_i(x, y)} \quad (11)$$

$f_i(x, y)$ is the gray-level value of pixel p in the material region x_i is the corresponding x-coordinate of p and y_i is the y-coordinate of it.

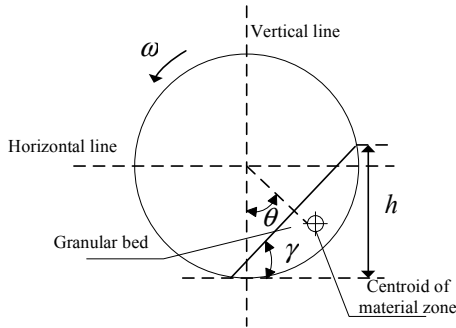


Fig. 8. Schematic diagram of granular material transport.

D. Outliers in Feature

We record a typical working condition of 10 minutes from an industrial alumina rotary kiln with a digital video camera, which at a frame rate 12 frame per second. The computer captures 7200 frames of stuff motion automatically. It is in the normal sintering state with the first 5-minute (about 1-3500 frame) and in undersintering state with the latter 5-minute (3501-7200) labeled by kiln operator expert.

The value of feature f_3 during this period is shown in Fig.9. The x-axis of table presents the frame number and y-axis presents the detected value. We can see it varies drastically at 1-3500 around and fluctuation range gets narrow at 3500-7200. Fig. 10 shows the value of angle of Centroid swing. There are some outliers in feature sequence also.

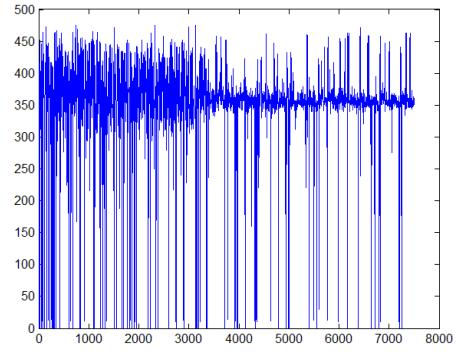


Fig. 9. Leftmost x-coordinate curve.

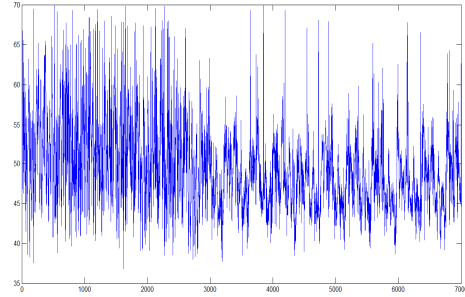


Fig. 10. Centroid swing angle curve.

There are some outliers in both of leftmost x-coordinate and centroid swing angle in Fig. 9. and Fig. 10.. These outliers exist because of the unsuccessful segmentation of material region. Due to the electromagnetic disturbance and dust of kiln, some images are blurring and the material region is difficult to be segmented. The unsuccessful segmentation results are shown in Fig. 11. To reduce influence of these outliers in features, we use a new classification algorithm to recognize the sintering state of material.

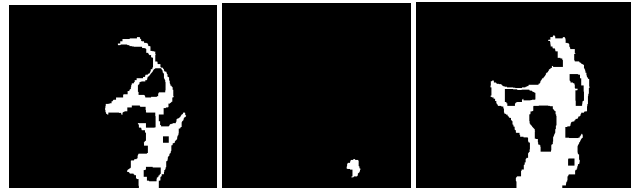


Fig. 11. Unsuccessful segmentation image.

III. CLASSIFIER FOR SINTERING STATE RECOGNITION

A. Background of Robust Neural Network

During the recent years, even though various learning algorithms have been studied in the literature [11]-[15], those approaches still suffer from the same problem such as slowly training speed, too many parameters need to be set and the complexity structure of methods. Unlike conventional neural network theories, a novel neural network architecture was used that in order to let single-hidden layer feed forward networks

work as an universal approximator. Such learning algorithm referred to as extreme learning machine(ELM) was proposed by Huang et al., which randomly generates hidden nodes and only need to adjust the output weights linking the hidden layer and the output layers[16]-[19]. ELM has the advantages of fast training speed, simple structure and superior universal approximation capability[20]-[22]. The network is obtained with very few steps and very low computational cost.

For N arbitrary distinct samples $(\mathbf{x}_i, \mathbf{t}_i)$, where $\mathbf{x}_i = [x_{i1}, x_{i2}, \dots, x_{im}]^T \in R^n$ and $\mathbf{t}_i = [t_{i1}, t_{i2}, \dots, t_{im}]^T \in R^m$, standard SLFNs with hidden nodes L and activation function $g(x)$ are mathematically modeled as

$$\mathbf{H}\boldsymbol{\beta} = \mathbf{T} \quad (12)$$

where

$$\mathbf{H} = \begin{bmatrix} g(\mathbf{a}_1 \cdot \mathbf{x}_1 + b_1) & \cdots & g(\mathbf{a}_L \cdot \mathbf{x}_1 + b_L) \\ \vdots & \cdots & \vdots \\ g(\mathbf{a}_1 \cdot \mathbf{x}_N + b_1) & \cdots & g(\mathbf{a}_L \cdot \mathbf{x}_N + b_L) \end{bmatrix}_{N \times L} \quad (13)$$

$\boldsymbol{\beta} = [\beta_1, \beta_2, \dots, \beta_L]^T \in R^{L \times d}$ is the weight vector connecting the i th hidden node and the output nodes. $\mathbf{T} = [\mathbf{t}_1, \mathbf{t}_2, \dots, \mathbf{t}_N]^T \in R^N$ is the output vector of samples. \mathbf{H} is hidden layer output matrix of neural network, the i th column of \mathbf{H} is the i th hidden node output with respect to inputs $\mathbf{x}_1, \mathbf{x}_2, \dots, \mathbf{x}_N$. Huang proved if the activation function $g(x)$ is infinitely differentiable, input weight vectors \mathbf{a}_i and hidden biases b_i are randomly chosen [23], $\boldsymbol{\beta}$ can be calculated directly in the following

$$\hat{\boldsymbol{\beta}} = \mathbf{H}^\dagger \mathbf{T} = (\mathbf{H}^T \mathbf{H})^{-1} \mathbf{H}^T \mathbf{T} \quad (14)$$

B. Robust ELM

ELM has the advantages of fast training speed and simple structure, but the generalization performance still may be destroyed by the unstable, high-disturbance learning data. Horata[24] proposed three algorithm, i.e. the iteratively reweighted least squares, ELM based on the multivariate least-trimmed squares, and ELM based on the one-step reweighted to solve the outliers robustness problem. As discussed above, there are many outliers in the training data because of the unstable segmentation results of flame image, which would reduce the generalization performance of neural networks. In this section, to deal with the corrupted data by outliers in industrial field, we use RB-ELM (Robust extreme learning machine) to recognize the sintering state.

1) calculating $\boldsymbol{\beta}$ by M-estimator

The SLFNs model, (12), is redefined as

$$\mathbf{H}\boldsymbol{\beta} = \mathbf{T} + \mathbf{e} \quad (15)$$

Where residuals error vector $\mathbf{e} = [e_1 \ e_2 \ \dots \ e_N]$ and $e_i = \mathbf{t}_i - \sum_{j=1}^L h_{ij} \beta_j$ is the i th sample's error. The traditional least square method is to minimize the residual sum of squares with the following cost function :

$$Q = \sum_{i=1}^N e_i^2. \quad (16)$$

The above cost function, such as (16), easily amplifies the influence of abnormal values(outliers) for system estimation because of the error square. The basic idea of M-estimator [25] is that using iterative weight least square to estimate regression coefficient $\boldsymbol{\beta}$, and determining samples weight by the size of residuals. In order to alleviate the outlier problem, M-estimators are used as the cost function of the networks in this paper. An M-estimator is of the following form according to (16):

$$Q = \sum_{i=1}^N \rho(e_i) \quad (17)$$

Where ρ is the kernel function which has the lower order than square. In order to minimize the Q with $\boldsymbol{\beta}$, the partial derivative of cost function with respect to $\boldsymbol{\beta}$ is

$$\sum_{i=1}^N \psi(\mathbf{t}_i - \sum_{j=1}^L h_{ij} \beta_j) h_{ij} = 0 \quad (18)$$

where ψ is the derivative function of ρ ($\psi = \rho'$), if making $w_i = w(e_i) = \psi(e_i)/e_i$, then the (18) conversion to $\sum_{i=1}^N w_i \mathbf{H}_i e_i = 0$. Its vector representation is :

$$\mathbf{H}^T \mathbf{W} \mathbf{e} = \mathbf{0} \quad (19)$$

Where $\mathbf{W} = \text{diag}(w_1, w_2, \dots, w_N)$ is the error weighted matrix and $w_i = w(e_i) = \psi(e_i)/e_i$ is the i th sample's error weight. Substitute (15) into (19), we can obtain the final estimating equation. That is

$$\boldsymbol{\beta} = (\mathbf{H}^T \mathbf{W} \mathbf{H})^{-1} \mathbf{H}^T \mathbf{W} \mathbf{Y} \quad (20)$$

Equation (20) is an equation of weighted least squares estimation. In order to reduce the inference of outliers, the weight of each sample is determined by the residual. Given a higher weight to a smaller residual sample, and given a lower weight to a larger residual sample. Then calculate each new residual by the given weight, iterative again and again, until the

change of weight coefficient is less than a certain allowable error. In this way, the robustness property of algorithm is enhanced.

2) selection of kernel functions

In the theory of M-estimator, there are many kernel functions ρ in (17). In this paper, we select Huber kernel function to substitute the residual sum of squares Q , such as

$$\rho(x) = \begin{cases} x^2/2 & |x| \leq k \\ k|x| - k^2/2 & |x| > k \end{cases} \quad (21)$$

Where k is a tuning constant, the default value is 1.345.

The derivative function of $\rho(x)$ is $\psi(x)$

$$\psi(x) = \begin{cases} -k & x < -k \\ x & |x| \leq k \\ k & x > k \end{cases} \quad (22)$$

3) normalizing error

In order to enhance the robustness of M-estimator, a robust scale estimate is used to standardize the error w_i in weighed matrix W . The value of s is defined as $med(|e_i|)/0.6745$. So, the standardized residual is defined as

$$u_i = e_i / s = 0.6745e_i / med(|e_i|) \quad (23)$$

where med means MAD (median absolute deviation). So the i th sample's error weight is redefined as

$$w_i = \frac{\psi(u_i)}{u_i} \quad (24)$$

Where $\psi(x)$ and u_i are defined by (22) and (24) respectively.

C. Procedure of RB-ELM Algorithm

Given a training set $Z = \{(x_i, t_i) | x_i \in R^n, t_i \in R^m, i = 1, 2, \dots, N\}$, activation function $g(x)$, and hidden node number L .

- a) Randomly assign input weight a_i and bias b_i , $W=I$, $\hat{\beta}^{(0)}=0$.
- b) Calculate the hidden layer output matrix H .
- c) Calculate the initialized output weight $\hat{\beta}^{(i)} = (H^T W H)^{-1} H^T W T$, and calculate the initialized individual error e ;
- d) **If** $\max(|\hat{\beta}^{(i)} - \hat{\beta}^{(i-1)}|) \geq \varepsilon$ **then**,

updating the error weight matrix $W = \text{diag}(w_1, w_2, \dots, w_N)$ with calculating the standardized residual u_i and $w_i = \frac{\psi(u_i)}{u_i}$ and then back to step c)

Else

algorithm finished and output the latest $\hat{\beta}^{(i)}$.

end if.

IV. EXPERIMENTS

In this paper, the original flame images were picked out from the flame's monitor video of No. 6 rotary kiln at the ZhongZhou Aluminum Corporation in China. We extracted the frame at a rate of 1 frame per minute and labeled its sintering state as undersintering images, normal sintering images or oversintering images by kiln worker expert. Training set has a total of 4500 typical flame images and testing set has 2000 images with three kinds of sintering states. We extracted the features from preprocessed image and each image is characterized by a vector in a 5-D feature according to (5)-(11). The information of Kiln data is shown in Table I and the testing results are shown in Table II.

The images with 5-D feature are classified by the RB-ELM mentioned in section III. The classification result of RB-ELM is shown in Table II. Meanwhile other classified algorithms are compared to the RB-ELM and the experiment results are listed in Table II. The total time required to process a single image is less than approximately 30 seconds, running on a PC with an Intel Dual-Core CPU at 2.60 GHz and 2 GB of RAM. The recognition test time of RB-ELM and ELM are less than BP and SVM.

TABLE I. INFORMATION OF KILN DATA

Training	Testing	Attributes	Classes
4500	2000	5	3

Table II shows that the recognition accurate rates of RB-ELM, ELM and SVM are more than 80%, which demonstrates the effectiveness of image processing procedure and 5-D features chosen in this paper. The test result of RB-ELM is better than ELM, SVM and BP, which shows that the RB-ELM can solve the outlier problem in feature data better than other learn machines.

We update the existing expert control system with the above sintering process recognition methods in this paper for a rotary kiln in ZhongZhou Aluminum Corporation in China. The updated control system could take different strategy according to the recognition result, which achieved a great quality improvement of final production. The results are shown in table III. Before we used the expert control system, the average quality rate was 63.1% and it raised to 87.5% when we apply the automation control system in rotary kiln.

TABLE II. THE COMPARISON OF PERFORMANCE OF ROBUST-ELM, ELM AND SVM

	Time(S)		Accuracy (%)		Number of hidden nodes
	Training	Testing	Training	Testing	
RB-ELM	0.6319	0.0253	79.43	81.17	100
ELM	0.2431	0.0288	79.30	80.91	100
SVM	3.2031	0.5938	79.55	81.05	C=32,g=32
BP	6.553	0.412	76.23	75.03	50

TABLE III. THE COMPARISON OF QUALITY RATES OF AUTOMATION CONTROL SYSTEM AND MANUAL CONTROL IN NO.6 ROTARY KILN

	Automation control	Manual control
Average quality rate(%)	87.5	63.1

V. CONCLUSION

Sintering state is important for the sintering quality of material in rotary kiln. The digital image captured in sintering area can assist in estimating the sintering state of material.

However, material region's segmentation of blurring image is difficult because of the disturbance of field environment. This paper proposes a novel method to recognize the sintering state of material in the rotary kiln based on RB-ELM (robust extreme learning machine), being the feature vector representing each image composed of gray-level statistic features. Firstly, preprocessing procedures such as illumination compensation and background homogenization are carried out to balance the image illumination. Secondly, material region is segmented by region growing algorithm. Then a 5-D feature vector based on grey-level statistic is extracted from segmented image. Finally the features are put into a RB-ELM to classify the sintering state. RB-ELM can effectively reduce the interference of outliers and noisy data. From the simulation results, for some cases, RB-ELM proved the superior robust capacity to ELM, and it still keeps the rapidity of ELM. Field experiment results show that the proposed approach in this paper can recognize the sintering state of material in rotary kiln effectively.

REFERENCES

[1] R. J. Spurling, J. F. Davidson, and D. M. Scott, "The transient response of granular flows in an inclined rotation cylinder," *Chemical Engineering Research and Design*, vol. 79, pp. 51-61, 2001.

[2] B. Lin, and S. B. Jørgensen, "Soft sensor design by multivariate fusion of image features and process Measurements," *Journal of Process Control*, vol. 21, pp. 547-553, 2011.

[3] P. Sun, T. Y. Chai, and X. J. Zhou, "Rotary Kiln Flame Image Segmentation Based on FCM and Gabor Wavelet Based Texture Coarseness," *Proceedings of the 7th World Congress on Intelligent Control and Automation, Chongqing, China*, pp. 7615-7620, 2008.

[4] M. He, J. Zhang, M. Yan, and H. Chen, "Texture Analysis and Classification for Clinker in Rotary Kiln," *OPEE 2010-2010 International Conference on Optics, Photonics and Energy Engineering*, vol. 1, pp. 211-214, 2010.

[5] H. L. Zhang, X. T. Chen, Z. Zou, and J. Li. "Content-based Rotary kiln Flame Image Retrieval," *Proceedings-1st International Congress on Image and Signal Processing*, vol. 2, pp. 490-494, 2008.

[6] W. T. Li, D. H. Wang, and T. Y. Chai, "Flame Image-Based Burning State Recognition for Sintering Process of Rotary Kiln Using Heterogeneous Features and Fuzzy Integral," *IEEE Transactions on industrial informatics*, vol. 8, pp. 780-790, 2012.

[7] J. C. Bezdek, "Pattern Recognition with Fuzzy Objective Function Algorithm," New York: Plenum Press, 1981.

[8] R. C. Gonzalez, and R. E. Woods, "Digital Image Processing," Second ed., Prentice Hall, New York, 2002.

[9] H. Henein, J. K. Brimacombe, and A. P. Watkinson, "Experimental study of transverse bed motion in rotary kilns," *Metallurgical Transactions B*, vol. 14B, pp. 191-205, 1983.

[10] P. Tegzes, T. Vicsek, and P. Schiffer, "Avalanche dynamics in wet granular materials," *Physical Review Letters*, vol. 89, pp. 943011-943014, 2002.

[11] D. S. Chen, and R. C. Jain, "A robust back propagation learning algorithm for function approximation," *IEEE Transaction on Neural Networks*, vol. 5, pp. 467-479, 1994.

[12] C. C. Chung, S. F. Su, C. C. Hsiao, "The annealing robust backpropagation(ARBP) learning algorithm," *IEEE Transactions on Neural Networks*, vol. 11, pp. 1067-1077, 2000.

[13] C. C. Lee, P. C. Chuang, J. R. Tsai and C. I. Chang, "Robust radial basis function neural networks," *IEEE Transaction on Systems, Man, and Cybernetics. Part B*, vol. 29, pp. 674-685, 1999.

[14] H. L. Shieh, Y. K. Yang, P. L. Chang, and J. T. Jeng, "Robust neural-fuzzy method for function approximation," *Expert Systems with Applications*, vol. 36, pp. 6903-6913, 2009.

[15] T. Moumen, E. Melegy, "Random Sampler M-Estimator Algorithm With Sequential Probability Ratio Test for Robust Function Approximation via Feed-Forward Neural Networks," *IEEE Transactions on Neural Networks and Learning Systems*, vol. 24, pp. 1074-1085, 2013 .

[16] G. B. Huang, Q. Y. Zhu, and C. K. Siew, "Extreme learning machine: a new learning scheme of feedforward neural networks," *IEEE International Conference on Neural Networks-Conference Proceedings*, vol. 2, pp. 985-990, 2004.

[17] G. B. Huang, "Learning capability and storage capacity of two-hidden-layer feedforward networks," *IEEE Transactions on Neural Networks*, vol. 14, pp. 27-281, 2003.

[18] Y. M. Yang, Y. N. Wang, and X. F. Yuan, "Bidirectional extreme learning machine and its learning effectiveness," *IEEE Transactions on Neural Networks and Learning Systems*, vol. 23, pp. 1408-1505, 2012.

[19] Y. M. Yang, Y. N. Wang, and X. F. Yuan, "Parallel chaos search based incremental extreme learning machine," *Neural Processing Letters*, vol. 37, pp. 277-301, 2013.

[20] G. B. Huang, L. Chen, and C. K. Siew, "Universal Approximation Using Incremental Constructive Feedforward Networks with Random Hidden Nodes," *IEEE Transactions on Neural Networks*, vol. 17, pp. 879-892, 2006.

[21] G. B. Huang, and L. Chen, "Convex Incremental Extreme Learning Machine," *Neurocomputing*, vol. 70, pp. 3056-3062, 2007.

[22] G. B. Huang, and L. Chen, "Enhanced Random Search Based Incremental Extreme Learning Machine," *Neurocomputing*, vol. 71, pp. 3460-3468, 2008.

[23] G. B. Huang, Q. Y. Zhu, and C. K. Siew, "Extreme learning machine: theory and application," *Neurocomputing*, vol. 70, pp. 489-501, 2006.

[24] P. Horata, S. Chiewchanwattana, and K. Sunat, "Robust extreme learning machine," *Neurocomputing*, vol. 102, pp: 31-44, 2013.

[25] L. Catherine, J. B. Keats, and D. C. Montgomery, "Comparison of Robust and Least Squares Regression in Computer-Generated Probability Plots," *IEEE Transactions on Reliability*, vol. 46, pp. 108-115, 1997 .